How a second Mg^{2+} ion affects the phosphoryl transfer mechanism in a protein kinase: a computational study

Rodrigo Recabarren[a], Kirill Zinovjev[b], Iñaki Tuñón[c]* and Jans Alzate-Morales[a]*

[a] Centro de Bioinformática, Simulación y Modelado (CBSM), Facultad de Ingeniería, Universidad de Talca, 1 Poniente 1141, Talca, Chile.

[b] School of Biochemistry, University of Bristol, Biomedical Sciences Building, University Walk, Bristol, BS8 1TD, UK.

[c] Departament de Química Física, Universitat de València, Valencia, Spain.

* Corresponding authors

E-mail: jalzate@utalca.cl (J AM)

E-mail: ignacio.tunon@uv.es (I T)

Abstract

Mg^{2+} ions are essential for the proper functioning of protein kinases and their roles in kinase activity have been studied for years. However, recent investigations have shed new light into how these metal cofactors modulate the catalytic activity, and new functions for them have been assigned. As an example, it has been found that in CDK2 (cyclin-dependent kinase 2), an enzyme that had been postulated to work efficiently with only one Mg^{2+} ion, a second Mg^{2+} ion needs to be bound in the active site for achieving an optimal catalytic performance. Thus, in this contribution, the phosphoryl transfer reaction in CDK2 has been studied in detail considering the presence of an additional Mg^{2+} ion in the active site. For this purpose, QM/MM (quantum mechanics/molecular mechanics) free energy calculations with the adaptive string method were performed, which showed that indeed the system containing two Mg^{2+} ions exhibits a lower activation free energy, corroborating the experimental observations. Structural and electronic analyses helped to identify the main factors that explain the differences in reaction barriers, giving a special emphasis to the reduced electrostatic repulsion that is felt by the reacting fragments when two Mg^{2+} ions are present in the active site. On the other hand, it was confirmed that the base-assisted mechanism is favored over the substrate-assisted pathway in the presence of two Mg^{2+} ions. The role of Asp127 was clarified; therefore, this residue acts firstly as a catalytic base and then as a catalytic acid protonating the transferred phosphoryl group. It is expected that these results may be extrapolated to other structurally related kinases where the influence of a second Mg^{2+} ion within the active site is still under debate.

1. Introduction

Phosphoryl transfer reactions are ubiquitous in all biological systems and their capacity to be regulated allow signaling and metabolic cascades to exist.[1] Protein kinases catalyze phosphorylation reactions that regulate a wide range of biological events, such as carbohydrate and lipid metabolism, neurotransmitter biosynthesis, DNA transcription and replication, organelle trafficking, smooth muscle contraction, cell differentiation, among others.[2] The phosphoryl transfer reaction catalyzed by protein kinases is helped by specific residues and Mg^{2+} cofactors within the active site, which allow a proper positioning of the substrates and stabilize the negative charges at the active site, respectively.[2,3] Besides, the presence of divalent metals affects nucleotide binding and the phosphoryl transfer step[2,4–6]. Here, all protein kinases appear to be able to bind two Mg^{2+} ions[2]; however, while in some cases the binding of two Mg^{2+} ions in the active is favorable for catalysis,[7–9] in other cases, e.g. in early studies of cyclic AMP-dependent protein kinase A (PKA),[10–12] it was observed that the binding of a second Mg^{2+} ion produced an inhibitory effect.

In this context, cyclin-dependent kinase 2 (CDK2) is a very interesting system to study since it was first suggested that this enzyme operates with only one Mg^{2+} ion in its active site,[13] but later it was found that two metal cofactors are indeed needed for optimal catalytic activity.[6,14] CDKs phosphorylate peptide substrates at either serine or threonine residues using ATP (adenosine triphosphate) as a phosphate source.[15] Their names come because, in order to be fully activated, CDKs need to be bound to a cyclin protein partner,[16–18] and they also need to be phosphorylated at specific residues[19–23] (Thr160 in CDK2,[24] see Fig. 1A). CDKs are well known as important regulators of the eukaryotic cell cycle; however, many other biological functions have been recently discovered,[25,26] and CDKs in higher eukaryotic cells arise as important regulators of transcription, metabolism and cell differentiation. Thus, and mainly due to their studied roles in the cell cycle, they have become very attractive therapeutic targets, especially for cancer treatment.[27–29] Unfortunately, despite extensive research in this area, rather unsatisfactory

results have been obtained so far, and therefore new strategies for their inhibition are sought.[30] At this point, the precise knowledge of the reaction mechanisms in CDKs could help to propose new molecular hypotheses for speeding up the development of more potent and selective drugs.

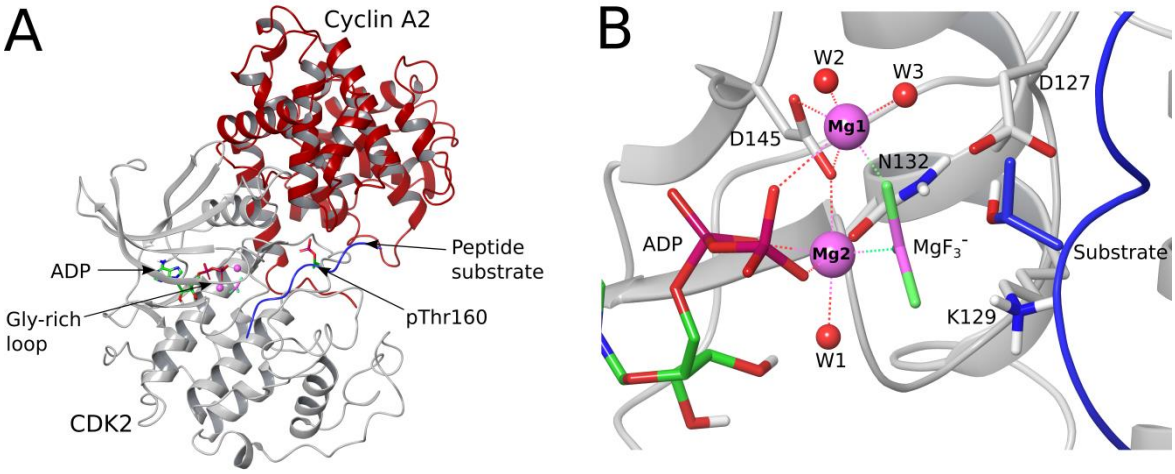

Figure 1. (A) Overall fold of the transition state mimic complex CDK2/Cyclin A2 with a 10-residue peptide substrate (blue) indicating the position of ADP, the glycine-rich loop and the phosphorylated residue pThr160 (PDB ID: 3QHW). (B) Active site close-up view labeling residues Asp127, Lys129, Asn132, Asp145 and the substrate threonine, together with ADP, the MgF_3^- molecule, magnesium ions and coordinating waters. Dashed lines represent the coordination spheres of both Mg1 and Mg2 ions.

As mentioned previously, the use of Mg^{2+} ions as cofactors in protein kinases is essential for their proper functioning, but a detailed molecular description of how Mg^{2+} ions work within the active site of these enzymes has not been provided yet. The ATP molecule in the cell is always coordinated by one Mg^{2+} ion (ATP-Mg), which is the substrate complex in most protein kinases.[31] This ion corresponds to Mg2 in the active site according to the nomenclature used in protein kinases[2] (see Fig. 1B), and it is coordinated in CDK2 by two non-bridging oxygen atoms from the α- and γ-phosphates of ATP, one β-γ bridging oxygen, Asn132, Asp145 and a water molecule, completing in this way an octahedral coordination[32] (Fig. 1B). The binding site for this Mg^{2+} ion is the one that had been found occupied previously in

CDK2 crystals,[4,13,32] and therefore, until just recently, the phosphoryl transfer mechanism in CDK2 had been described involving only that single Mg^{2+} ion (1-Mg system).[33–36] However, Bao *et al.*[6] obtained a crystallographic structure of a pCDK2/Cyclin A transition state complex mimic with a second Mg^{2+} ion (Mg1) bound within the active site, showing that CDK2 most probably works with two Mg^{2+} ions as cofactors (2-Mg system). In this structure, the second ion is coordinated by a β-phosphate oxygen from ADP and a fluorine atom from the transition state (TS) mimic MgF_3^-, which would be representing a γ-phosphate oxygen if ATP was present in the active site; in a bidentate coordination by Asp145, and two water molecules (Fig. 1B). This second Mg^{2+} ion (Mg1) occupies the binding site that was known to be filled in protein kinases like PKA,[37] thus suggesting a common catalytic mechanism in both enzymes. In the crystallographic and kinetic study of Bao *et al.*[6], and in subsequent ones by the same authors,[14] they show that Mg1 has a transient nature, since it is expelled from the active site after the phosphoryl transfer step has been completed to allow for the release of ADP, but its presence was found to be necessary for achieving maximum rate enhancement of the chemical reaction.[6,14] Interestingly, a similar mechanism has been proposed for PKA, alluding to be a more general mechanism in protein kinases.[38] One relevant structural feature of the 2-Mg system, when compared with previous 1-Mg crystallographic structures, is the conformation of the glycine-rich (Gly-rich) loop, a structural motif that functions as a lid closing the active site.[3] This loop is found in more open conformations in crystals with only one metal ion (at Mg2 position),[4,13,32] while it is found in a closed conformation in the crystal structure with two Mg^{2+} cofactors.[6] Besides, it has been observed by means of molecular dynamics (MD) simulations that the 2-Mg system was much more rigid than the 1-Mg system, indicating a structural stabilization role for Mg1.[6]

The phosphoryl transfer reaction can take place through three main reaction pathways:[39] one in which the reaction goes through a dissociative mechanism involving a metaphosphate intermediate, characterized by advanced dissociation between the leaving oxygen and the γ-phosphorus atom; a second option is an associative mechanism involving a pentavalent phosphorane intermediate, where

bond formation with the entering oxygen is more advanced than dissociation with the leaving oxygen; and a third scenario featuring a concerted mechanism, i.e., with only one transition state. Here, the nature of the transition state could also be more dissociative or associative, for which the terms “loose” or “tight” are also used, respectively.[39] Other important feature in the mechanism is the activation step (deprotonation) of the serine/threonine residue to accomplish its phosphorylation. It has been proposed that Asp127 in CDK2 may serve as a catalytic base abstracting the hydroxyl proton, allowing the consecutive phosphorylation of the substrate residue.[32] This mechanistic route is therefore called base-assisted mechanism (Fig. 2), and features in principle, a dissociative-like mechanism.[35,40,41] Moreover, it is plausible to think that this mechanism involves a last protonation step (step 2 in Fig. 2), which has been studied in protein kinases like PKA, where the protonated aspartic acid residue (Asp166 in PKA) delivers back the proton to one of the oxygen atoms of the transferred phosphoryl group.[40,42] Having a protonated phosphate group at the phosphorylation site would in turn help to destabilize its interaction with the Mg^{2+} ions, favoring its release from the active site.[43] On the other hand, the substrate hydroxyl proton could be abstracted by one γ-phosphate oxygen atom, route called substrate-assisted mechanism (Fig. 2), which usually resembles a more associative-like mechanism.[34,40]

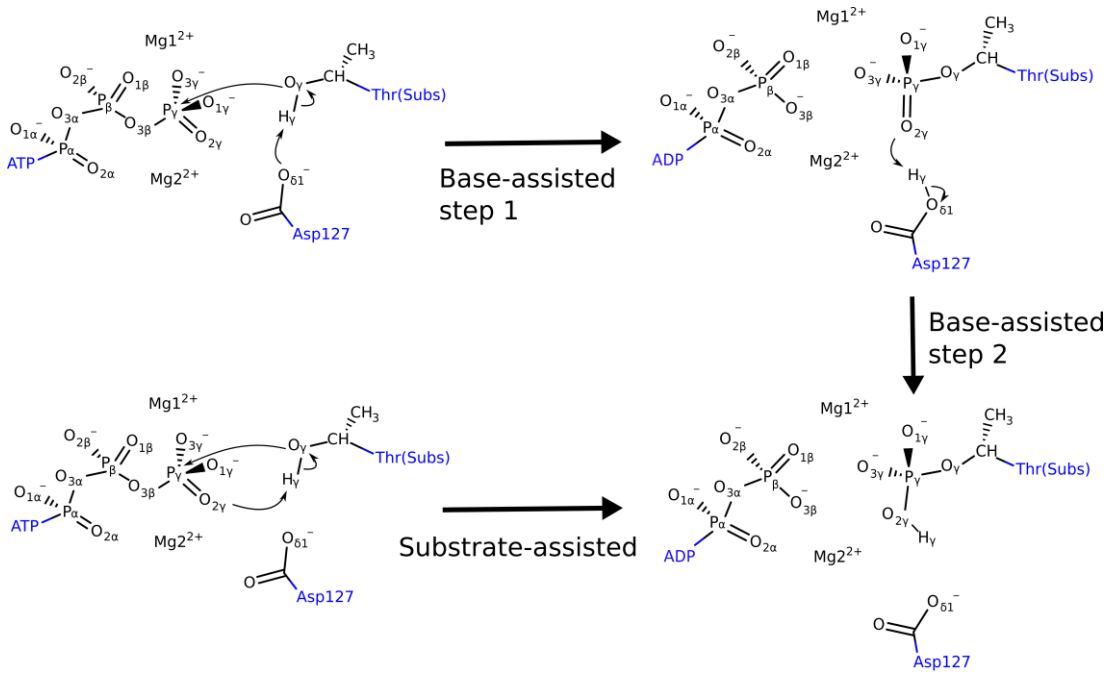

Figure 2. Base-assisted and substrate-assisted pathways for the phosphoryl transfer reaction in CDK2. The base-assisted mechanism may involve a second step where the proton is transferred from the external base (Asp127) to one phosphoryl oxygen ($O_{2\gamma}$ in this case) generating the same product as the substrate-assisted route.

Computational studies on non-enzymatic and enzymatic phosphoryl transfer reactions are vast in the literuature;[1,44–47] however, computational studies in kinases have been rather limited.[1] With respect to CDK2, the first computational study used QM cluster calculations at a DFT (density functional theory) level and pointed to a substrate-assisted mechanism with an estimated energy barrier of 42 kcal/mol,[33] clearly above the experimental estimations (15.3 kcal/mol from k_3= 35 s^{-1} [24] using transition state theory). Some of the same authors performed later a QM/MM study, where they also proposed the substrate-assisted mechanism as the operating one with an energy barrier of 24 kcal/mol, attributing only a structural role for Asp127.[34] A subsequent QM/MM study by Smith *et al.*[35] proposed a concerted base-assisted mechanism with a loose transition state as the most favorable one (free energy barrier of 10.8 kcal/mol), while they observed an energy barrier over 30 kcal/mol for the substrate-assisted mechanism. However, the best estimation of the free energy barrier was somewhat lower than the experimental derived value (15.3 kcal/mol). The authors argued that the different experimental conditions such as the nature of the peptide substrate with which the values were compared could be a potential source of error. A more recent QM/MM study analyzing the potential energy surface (PES) of the reaction performed in our group also reaffirmed that the base-assisted mechanism is more favorable than the substrate-assisted one.[36] These last results agreed with computational studies in PKA[40–42,48,49] and in other kinases,[50,51] which also point to a base-assisted mechanism with a strong dissociative character as the operating one, though the substrate-assisted mechanism has been proposed as the most favorable in other kinases.[52,53]

Despite the numerous experimental and computational studies performed in CDK2, there is no clear understanding on how much a second Mg^{2+} ion would affect the phosphoryl transfer mechanism and its associated free energy barrier. Here, it is worth noting that all computational studies in CDK2 have considered only one Mg^{2+} ion within the active site,[33–36] and therefore that information is lacking. On the other hand, it is also interesting that some computational studies in other kinases have also shown that two Mg^{2+} ions within the active site appear to be important for transition state stabilization and hence lowering of the activation energy,[48,54] while others have suggested that a second Mg^{2+} ion would have a destabilizing effect on the transition state.[55,56] Therefore, a comprehensive study of the different structural motifs that could drive these observations is still needed.

The main goal of the present study is to assess the phosphoryl transfer mechanism in CDK2 using one of the most recent crystallographic structures that contains two Mg^{2+} ions in the active site and to estimate the free energy barrier of the chemical step, using also a model with only one Mg^{2+} ion for comparison purposes. To achieve this, QM/MM MD calculations have been performed, including in this way the direct effect of the protein environment and its flexibility on the quantum chemical calculations. Also, analyses of structural and electronic properties have been carried out to rationalize the differences between both modeled systems. It is expected that these results may help in obtaining a more profound understanding on how Mg^{2+} cofactors modulate phosphoryl transfer reactions in protein kinases.

2. Methods

2.1 System preparation and classical MD simulations

The CDK2/Cyclin protein complex model was built based on the crystal structure with PDB code 3QHW.[6] This structure contains the CDK2/Cyclin A2 protein complex bound to ADP, the TS mimic molecule MgF_3^-, a peptide substrate with primary sequence PKTPKKAKKL and two Mg^{2+} ions within the active site (Fig. 1B). The chains A, B and J were chosen for CDK2, cyclin and the 10-residue peptide

substrate, respectively. The MgF_3^- mimic was replaced by the γ-phosphate to build the ATP molecule in the reactant complex. This was done by aligning the protein structure to a previous crystal structure of CDK2 where the ATP molecule is present (PDB ID 1QMZ).[32] The product complex, where the ATP γ-phosphate has been transferred to the threonine residue of the peptide substrate, was built manually considering reported conformations of the transferred phosphoryl group in the product state of PKA.[40] Here, different states for the products were taken into account, i.e., one in which the transferred hydroxyl proton resides on Asp127, what would be the product of step 1 in the base-assisted mechanism (Figure 2), and other states where the proton is located at the phosphoryl oxygens $O_{2\gamma}$ and $O_{3\gamma}$, representing the products of step 2 in the base-assisted mechanism or the substrate-assisted pathway. To model the different mechanisms in the 1-Mg system, Mg1 was removed from the reactant and product complexes. Subsequently, classical MD simulations of the 1-Mg and 2-Mg systems in both reactant and product states were run for 10 ns. Additional details about the preparation of the systems, parameters assignment, minimization and equilibration are described in the Supporting Information (SI) section.

2.2 QM/MM free energy calculations

The last frame from MD simulations of the reactant and product complexes for 1-Mg and 2-Mg systems was used for setting up QM/MM calculations. The QM region was comprised of active site residues Asp127, Lys129, Asn132, Asp145 together with the complete triphosphate moiety of the ATP molecule, the substrate threonine residue, and both Mg^{2+} ions (or one Mg^{2+} ion in case of 1-Mg system) with their respective coordinating water molecules (Fig. S1). QM/MM cuts were applied between β and α carbons of protein residues and valences were completed with hydrogen atoms (link atom approach[57,58]), making a total of 77 and 70 QM atoms (including link atoms) in 2-Mg and 1-Mg systems, respectively. QM atoms were treated with two semiempirical methods, namely DFTB3[59–62] (3OB/OPhyd variant[61]) and AM1/d-PhoT[63] (results for this Hamiltonian are described in the SI).

Both methods have been developed to treat phosphoryl transfer reactions and have been applied extensively to study enzymatic catalysis during recent years.[47,51,64–69] Parameters for DFTB3 simulations were kindly provided by Daniel Roston (UC San Diego).[61] The MM region was treated with the Amber ff99SB force field. Reactant and product complexes for both 1-Mg and 2-Mg systems were first subjected to QM/MM minimization calculations using the respective QM/MM potentials. Subsequently, QM/MM MD simulations were performed for 100 ps in NVT ensemble to equilibrate reactant and product conformations using a time step of 1 fs. Temperature was kept at 300 K by means of Langevin thermostat with a collision frequency of 1 ps^{-1}. All simulations were performed with the simulation package AmberTools17 using the *sander* module.[70]

Equilibrated structures of reactants and products for each mechanism were extracted to calculate the minimum free energy path (MFEP) that connects both states in a space of collective variables (CVs) using a modified version of the on-the-fly string method[71] (the adaptive string method, ASM[72]). Generally speaking, the string method[71,73] allows finding the MFEP by using a series of coupled restrained MD simulations connecting equidistant points along some path in the CV space that links reactants and products. These points, or nodes, move to the regions of lower free energy, converging to the MFEP.[74] In this way, the calculation of the complete free energy surface is not needed assuming that reactive trajectories rarely visit regions far from the MFEP. As in previous studies, the string method has been combined with the use of a path CV[75,76], *s* coordinate in this work, that measures the progress along the reaction. Umbrella sampling (US[77]) with Hamiltonian Replica Exchange[78] were used to sample the configurational space along this reaction coordinate and to obtain the corresponding potential of mean force (PMF). This approach has been successfully applied to different enzymatic reactions.[50,75,79–84]

Figure 3 shows the choice of the CVs for string method and path CV calculations. CVs 1 and 2 describe the breaking and formation of P-O bonds, respectively, while

CVs 3 and 4 represent the proton transfer from the threonine's hydroxyl group to Asp127. CV5 corresponds to a hybridization coordinate that measures the distance between the P_γ atom and the plane formed by the three phosphoryl oxygens $O_{1\gamma}$, $O_{2\gamma}$ and $O_{3\gamma}$. CVs 6 and 7 describe the donor-acceptor distances of the phosphoryl transfer and proton transfer reactions, respectively. CVs 8 and 9 describe the step 2 of the base-assisted mechanism that involves the proton transfer from Asp127 to the phosphoryl oxygen atom $O_{2\gamma}$ (Fig. 2). CV8 also helps to describe the direct proton transfer from the threonine's hydroxyl proton to the phosphoryl oxygen $O_{2\gamma}$ in the substrate-assisted pathway. Finally, CV10 is the distance Mg2 - $O_{2\gamma}$, which was included after observing that this distance was too elongated in the base-assisted mechanism in the 1-Mg system. The inclusion of this distance as a CV helps to keep the MFEP in the vicinity of those regions physically relevant. Step 2 of the base-assisted mechanism was only explored with the DFTB3 method after observing high free energy barriers when the AM1/d-PhoT Hamiltonian was used. In this way, the calculations using the AM1/d-PhoT Hamiltonian were studied with a smaller set of CVs (CV1-CV7). Finally, other phosphoryl oxygens were tested as proton acceptors in the substrate-assisted mechanism. For the sake of clarity, the CVs that were used for each string calculation are clearly depicted in the supporting information (SI). Other details of the string optimization and subsequent US calculations are provided in SI.

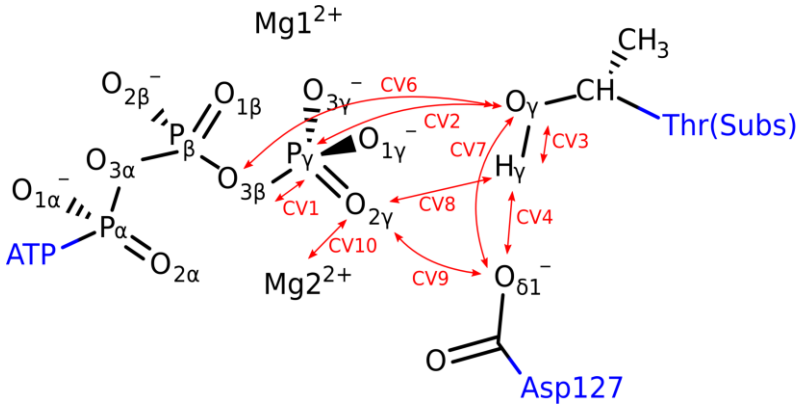

CV1	$O_{3\beta}$ - P_γ
CV2	P_γ - $O_{\gamma(Thr)}$
CV3	$O_{\gamma(Thr)}$ - $H_{\gamma(Thr)}$
CV4	$O_{\delta1(Asp127)}$ - $H_{\gamma(Thr)}$
CV5	P_γ-$O_{1\gamma}$-$O_{2\gamma}$-$O_{3\gamma}$
CV6	$O_{3\beta}$ - $O_{\gamma(Thr)}$
CV7	$O_{\delta1(Asp127)}$ - $O_{\gamma(Thr)}$
CV8	$O_{2\gamma}$ - $H_{\gamma(Thr)}$
CV9	$O_{\delta1(Asp127)}$ - $O_{2\gamma}$
CV10	Mg2 - $O_{2\gamma}$

Figure 3. Definition of the CVs used in the base-assisted and substrate-assisted mechanisms. All CVs correspond to simple distances except for CV5 which is a

hybridization coordinate defined by the distance between the atom P_γ and the plane formed by the three γ-phosphoryl oxygen atoms.

3. Results

3.1 Phosphoryl transfer mechanism with two Mg^{2+} ions

3. 1. 1. Base-assisted mechanism

In order to study the phosphoryl transfer mechanism in CDK2, MD simulations were performed to obtain relaxed structures of the reactant and product complexes with two Mg^{2+} ions. During the equilibration of the reactant complex using classical MD simulations, it was noticed that the hydroxyl group of the nucleophile threonine residue adopted different conformations; in some cases favoring a hydrogen bond (HB) interaction with Asp127 and in others favoring HBs with the γ-phosphate oxygens (Fig. 4A and B). To exemplify this, the HB distances with the different γ-phosphate and Asp127 oxygens are shown in Fig. 4A. It is therefore very clear that the thermal energy of the system is sufficient for generating this conformational change repeatedly during the simulation. This clearly indicates that, in principle, the threonine proton could be abstracted by the substrate ATP or by Asp127 and thus both proposed mechanisms would be plausible. This behavior was also observed in the QM/MM MD simulations performed at the DFTB3/ff99SB level (Fig. S2, see SI for a more detailed analysis).

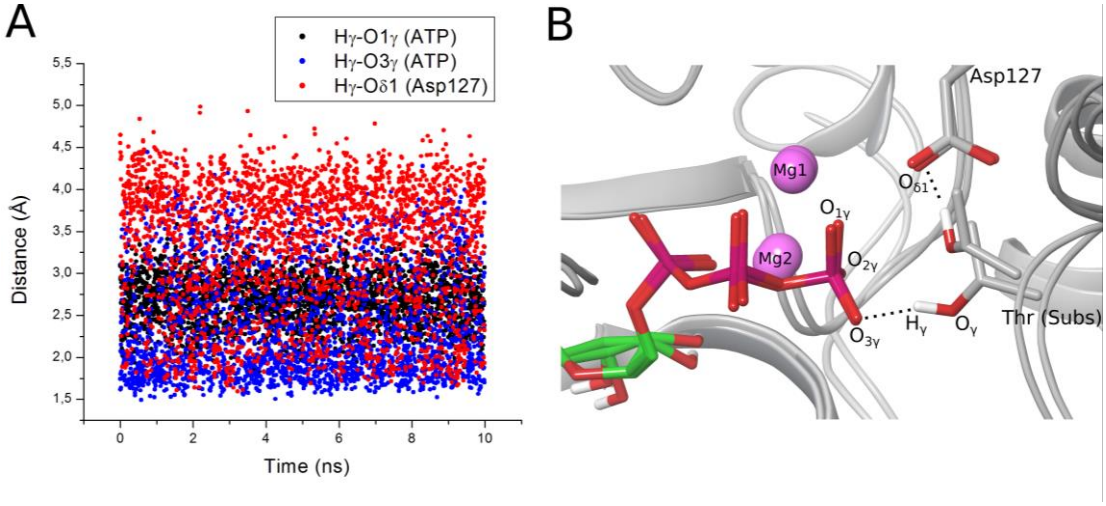

Figure 4. (A) Distances between the H_γ atom of the threonine's hydroxyl group with atoms $O_{1\gamma}$ and $O_{3\gamma}$ from the ATP molecule and the $O_{\delta 1}$ atom of Asp127 along a 10 ns MD simulation of the reactant state with two magnesium ions. (B) Superposition of the two last frames of the 10 ns MD simulation showing the different conformations that the threonine's hydroxyl group can adopt, and the respective hydrogen bonds formed (black dashed lines).

In this section we discuss the results corresponding to the mechanism where the target threonine is activated through proton abstraction carried out by Asp127. In the case of the DFTB3/ff99SB simulations, the product conformation used for the string calculations features the transferred phosphoryl group protonated at the $O_{2\gamma}$ oxygen (Fig. 2), which is still coordinating the Mg2 ion. Fig. 5 shows the calculated free energy profile at the DFTB3/ff99SB level of theory (Fig. 5A), together with the evolution of the CVs along the reaction coordinate *s* (Fig. 5B). In this case, the 10 CVs described in Fig. 3 were used to study the reaction mechanism. Information about the convergence of the string calculation is also provided in Fig. S3B. Although the initial values for the CVs in each node were set to favor a direct proton transfer from the threonine's hydroxyl group to the phosphoryl oxygen $O_{2\gamma}$, the string calculation converged to the base-assisted mechanism (see the evolution of CV4). The activation free energy amounts to 16.6 ± 0.5 kcal/mol, very close to the experimental estimation (15.3 kcal/mol).[24]

346 The most important CVs for this reaction are the ones that represent the breakage
347 and formation of P-O bonds (CV1 and CV2) and the respective proton transfer
348 reactions (CV3, CV4 and CV8). The reaction begins with an average distance for the
349 $O_{3\beta}$-P_γ bond (CV1) of 1.70 Å and of 3.45 Å for the P_γ-O_γ bond (CV2). The first event
350 observed is the gradual approach of the nucleophile $O_{\gamma(Thr)}$ atom towards P_γ,
351 represented by a decrease in CV2, whereas CV1 remains constant until a reaction
352 coordinate value of about 2.3 (units in $amu^{1/2}$·Å from hereafter). From this point,
353 CV1 keeps smoothly increasing while CV2 decreasing, showing the gradual
354 breakage of the $O_{3\beta}$-P_γ bond and the formation of the P_γ-$O_{\gamma(Thr)}$ bond, respectively,
355 until the first transition state (TS1a) is reached (Fig. 5 and 6B). Here, CV1 and CV2
356 take average values of 2.32 and 2.61 Å respectively, corresponding to a
357 metaphosphate-like transition state with high dissociative character (donor-
358 acceptor distance (CV6) of 4.93 Å). Following the reaction coordinate, an
359 intermediate state is found (IT1a), which is very close in energy to TS1, i.e, only 0.6
360 kcal/mol of difference. The IT1a intermediate (Fig. S4A) presents almost equal
361 values for CV1 and CV2, 2.51 Å and 2.46 Å, respectively, and with CV6 taking a
362 value 4.97 Å, reaffirming the dissociative character of the reaction. We pause here
363 to comment that this shallow intermediate is most probably due to a limitation of
364 the semiempirical Hamiltonian (the well is considerably deeper using other
365 parametrizations of the DFTB3 Hamiltonian, data not shown). In addition,
366 considering the sampling error, i.e., about 0.5 kcal/mol, this feature on the free
367 energy profile should be considered as kinetically irrelevant.

368

369 Advancing in the reaction, a second transition state is found (TS2a, Fig. 6C), which
370 is the highest point in the free energy profile (Fig. 5A). Here, CV1 and CV2 take
371 average values of 2.62 Å and 2.18 Å, respectively, showing that the phosphoryl
372 group is now much closer to the entering oxygen than to the leaving oxygen atom.
373 This process is accompanied by a shallow increase in the distance Mg2-$O_{2\gamma}$ (CV10),
374 as a result of the phosphoryl group transfer. The dissociative character of the
375 transition states can be assessed by using Pauling's formula as proposed by
376 Mildvan:[85] $D(n) = D(1) - 0.60\log(n)$, where $D(n)$ is the average value between the
377 two P-O distances, and $D(1)$ is the distance for a single P-O bond (1.73 Å). With

this, the fractional bond number (*n*) that gives an estimation of the associative/dissociative character of the TS can be estimated. In the case of TS1a, the fractional bond number is 0.06, which means that the TS is 6% associative (or 94% dissociative). In the case of TS2a, it has a dissociative character of 93%. Therefore, it is very clear that the TSs described at the DFTB3/ff99SB level exhibit a high dissociative character, which is expected for the base-assisted mechanism and agrees with other computational studies.[35,36,40]

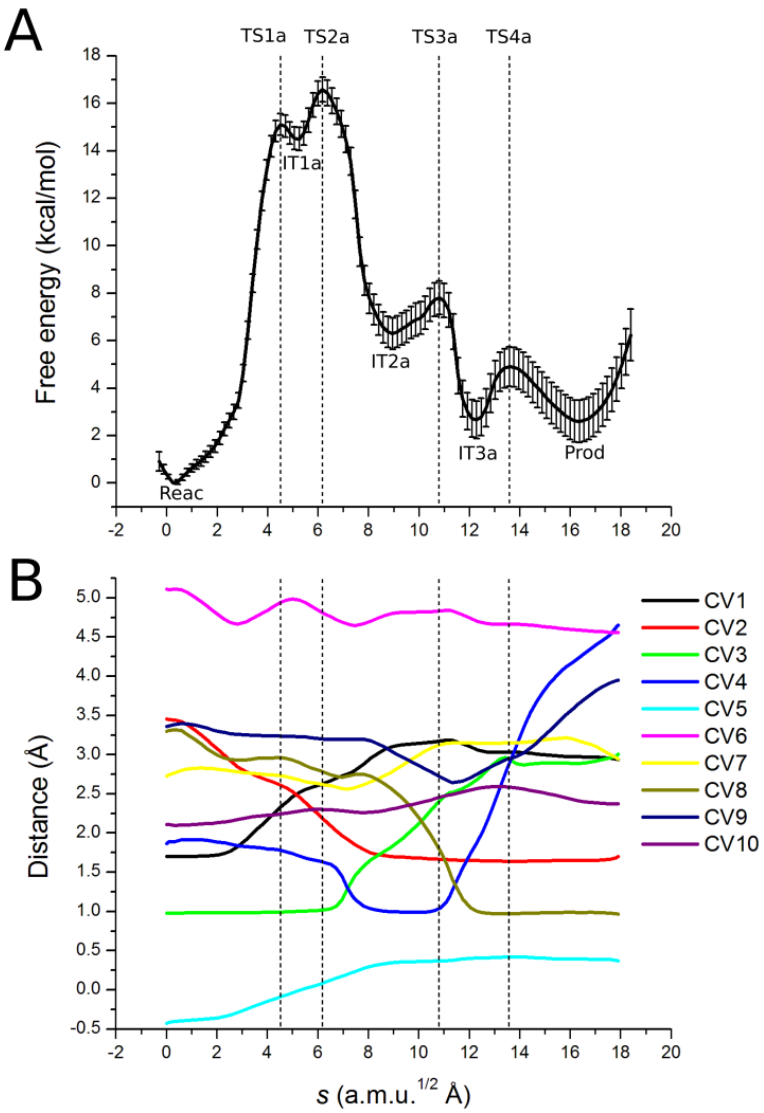

Figure 5. (A) Free energy profile for the base-assisted mechanism (steps 1 and 2) at the DFTB3/ff99SB level along the reaction coordinate *s* for the 2-Mg system. PMF calculated

over 90 ps of sampling in each window. Error bars correspond to 95% confidence intervals. Dashed vertical lines represent the positions of transition states TS1a, TS2a, TS3a and TS4a on the reaction coordinate. (B) Evolution of the CVs along the reaction coordinate *s*.

Just after TS2a, the first proton transfer reaction starts, as reflected in Fig. 5B by the elongation of the $O_{\gamma(Thr)}$-$H_{\gamma(Thr)}$ bond (CV3) and the simultaneous formation of the $O_{\delta1(Asp127)}$-$H_{\gamma(Thr)}$ bond (CV4). For this, the donor and acceptor oxygens get closer, as represented by a slight decrease in CV7 at the crossing point between CV3 and CV4 (CV7 ≈ 2.5 Å). Once the proton transfer reaction is completed at *s* value of 8.30 (CV4 ≈ 1 Å), the phosphoryl transfer is also completed, i.e., CV2 reaches a plateau representing the complete formation of the P_{γ}-$O_{\gamma(Thr)}$ bond. Thus, all these last processes generate a decrease in the free energy until a second intermediate state is formed (IT2a). This intermediate state features Asp127 protonated making a HB with the $O_{\gamma(Thr)}$ oxygen (Fig. S4B). From here, the free energy begins to increase again to reach a third transition state (TS3a, Fig. 6D). From Fig. 5, it is possible to see that the increase in the free energy is due to the approach of the oxygen $O_{\delta1(Asp127)}$ to the phosphoryl oxygen $O_{2\gamma}$, represented by a gradual decrease in collective variables CV8 and CV9. This event requires the breakage of the $O_{\delta1(Asp127)}$-$H_{\gamma(Thr)}$⋯ $O_{\gamma(Thr)}$ HB and rotation towards $O_{2\gamma}$, taking an approximate energy cost of 1.5 kcal/mol (energy difference between IT2a and TS3a).

Once an adequate conformation between the donor and acceptor oxygens is adopted at TS3a (CV9 = 2.72 Å, Fig. 6D), the proton transfer from Asp127 to the phosphate group occurs, which is accompanied by a decrease in the free energy, until a third intermediate state is reached (IT3a). IT3a features a protonated phosphate group at $O_{2\gamma}$ making a HB with the oxygen $O_{\delta1(Asp127)}$ (Fig. S4C). At this point, the distance between the protonated oxygen $O_{2\gamma}$ and Mg2 (CV10) is almost 2.6 Å, showing that the second proton transfer reaction alters the coordination of Mg2; however, the subsequent accommodation of the HB networks allows the recovery of the coordination at Mg2, though the final value for CV10 is almost 2.4

Å. Though IT3a could be considered the final product state of the phosphoryl transfer reaction, our QM/MM MD equilibration simulations reached to a conformation that is slightly different (see Fig. S5), where the HB $O_{2\gamma}$-$H_{\gamma(Thr)}\cdots O_{\delta1(Asp127)}$ has been broken and the protonated $O_{2\gamma}$ oxygen rotates away from Asp127 establishing a new HB with a water molecule. This last step is represented by a gradual increase in collective variables CV4 and CV9, which is the final free energy barrier in the profile at *s* value 13.6 (TS4a, Fig. 6E). This last rotation of the $O_{2\gamma}$-$H_{\gamma(Thr)}$ bond takes a free energy cost of 2.2 kcal/mol (energy difference between IT3a and TS4a). Here, the intermediate state IT3a and the final product state are almost isoenergetic, with the latter being only 0.7 kcal/mol more stable indicating that both conformations would be thermally accessible at the product state.

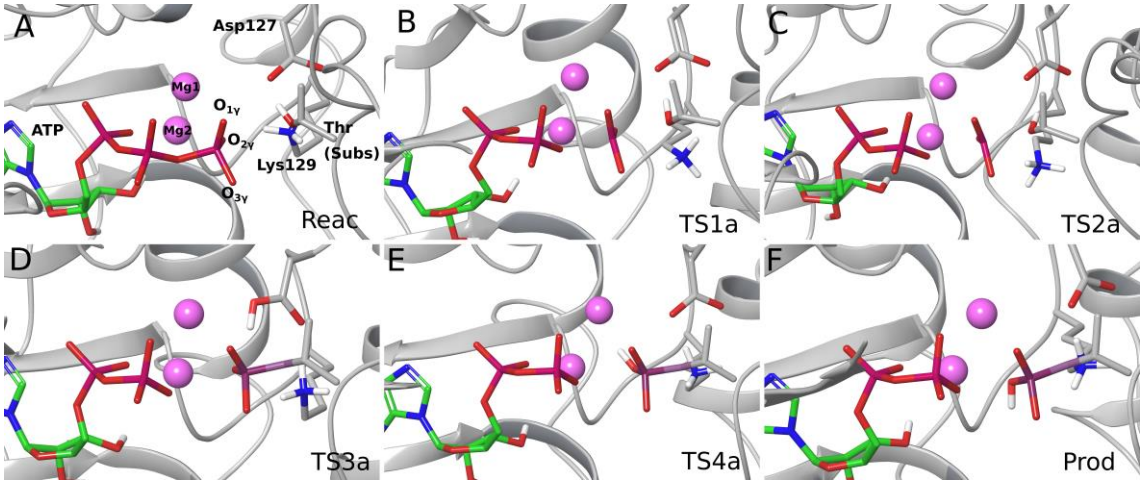

Figure 6. (A-F) Representative structures of reactants, transition states and products identified according to the free energy profile of Fig. 5A. The residue Lys129 is also shown in the structures to highlight its role in the stabilization of the γ-phosphoryl group through electrostatic and hydrogen bonding interactions.

Thus, the string method was able to capture the complete base-assisted mechanism (steps 1 and 2) showing that Asp127 acts firstly as a catalytic base and then as a catalytic acid protonating the transferred phosphoryl group. The proton transfer from the $O_{\gamma(Thr)}$-$H_{\gamma(Thr)}$ group to Asp127 occurs after TS2a has been

reached, and therefore contributes to the lowering of the free energy. The same is observed in the case of the second proton transfer step (TS3a). Interestingly, this is in agreement with QM/MM studies in PKA (PES scan using DFT for the QM region) where the same results have been found for the proton transfer steps.[40,41] Overall, the free energy barrier predicted at the DFTB3/ff99SB level (16.6 ± 0.5 kcal/mol) is in very good agreement with the experimental derived value for the activation energy (15.3 kcal/mol, k_3 = 35 s^{-1}).[24] On the other hand, calculations with the AM1/d–PhoT method reproduced a similar dissociative-like mechanism, though with a much higher free energy barrier (25.9 kcal/mol ± 1.0 kcal/mol). One of the main factors that explains this high free energy barrier is that AM1/d–PhoT predicts a too stable HB between the $O_{\gamma(Thr)}$-$H_{\gamma(Thr)}$ group and the phosphate oxygen $O_{3\gamma}$, generating an overestimated free energy penalty upon the rotation of the hydroxyl group towards Asp127. A more detailed analysis is given in the SI.

3. 1. 2. Substrate-assisted mechanism

The substrate-assisted mechanism (Fig. 2) was assessed with two Mg^{2+} ions in the active site at the DFTB3/ff99SB level using the reactant and product conformations previously used for the study of the base-assisted mechanism. Fig. 7 shows the free energy profile together with the CVs describing the reaction (see Fig. S6 depicting the convergence profile). It is readily seen that the free energy profile depicts a concerted mechanism (transition state TSc, dashed vertical line). The evolution of the CVs show how the reaction begins with the approach of $O_{\gamma(Thr)}$ to P_γ reflected by a continuous decrease in CVs 2 and 6. Subsequently, the $O_{\gamma(Thr)}$-$H_{\gamma(Thr)}$ bond is accommodated towards the right conformation to carry out the proton transfer to $O_{2\gamma}$, reflected by a decrease in CV8. Then, the $O_{3\beta}$-P_γ bond (CV1) begins to stretch until the transition state (TSc) is reached at *s* value of 7.10. At the transition state, CV1 and CV2 take average values of 1.91 and 1.92 Å, respectively, and therefore TSc corresponds to the point where both $O_{3\beta}$-P_γ and P_γ-$O_{\gamma(Thr)}$ distances are almost equal. Owing to the rather short P-O distances, and especially due to the well-advanced formation of the P_γ-$O_{\gamma(Thr)}$ bond, the TS has an associative character of 48%. As a result, the proton transfer to $O_{2\gamma}$ is well advanced at the transition state, with average values for CVs 3 ($O_{\gamma(Thr)}$-$H_{\gamma(Thr)}$) and 8 ($O_{2\gamma}$-$H_{\gamma(Thr)}$) of

1.59 and 1.19 Å, respectively. These values show that at the TS the bond $O_{\gamma(Thr)}$-$H_{\gamma(Thr)}$ is already broken and the bond $O_{2\gamma}$-$H_{\gamma(Thr)}$ is almost formed. The estimated free energy barrier is 26.2 ± 1.3 kcal/mol, which is considerably higher compared to the activation energy calculated for the base-assisted mechanism (16.6 ± 0.5 kcal/mol) and the experimentally derived value (15.3 kcal/mol).

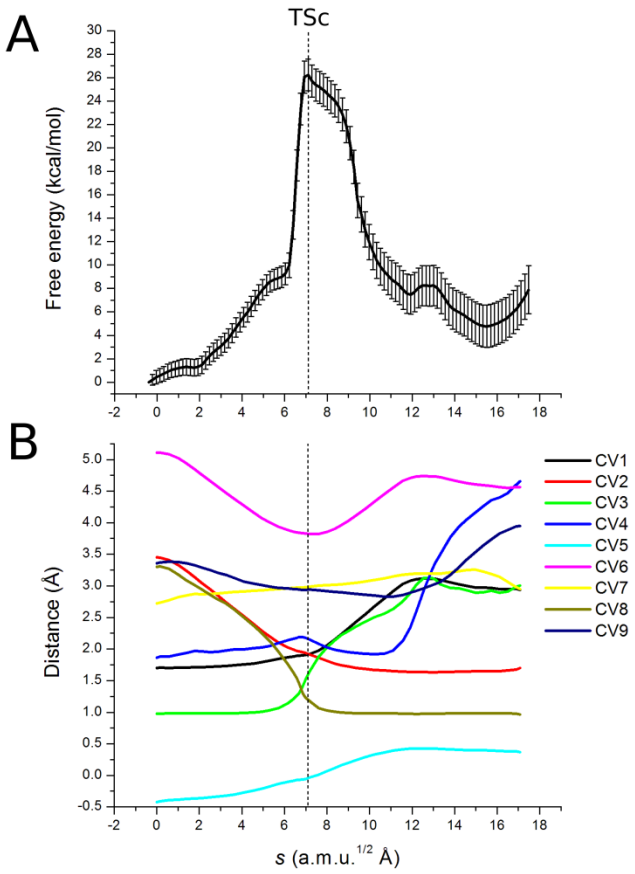

Figure 7. (A) Free energy profile for the substrate-assisted mechanism at the DFTB3/ff99SB level along the reaction coordinate *s* with 2 Mg^{2+} ions in the active site and with ATP oxygen $O_{2\gamma}$ as proton acceptor. PMF calculated over 20 ps of sampling in each window. Error bars correspond to 95% confidence intervals. Dashed vertical line represents the position of transition state TSc on the reaction coordinate. (B) Evolution of the CVs along the reaction coordinate *s*.

The reaction is completed with the total dissociation of the $O_{3\beta}$-P_γ bond, and the final formation of the P_γ-$O_{\gamma(Thr)}$ bond. The final small barrier observed at $s \approx 12.6$ is the rotation of the $O_{2\gamma}$-$H_{\gamma(Thr)}$ bond away from Asp127 as described in the base-

assisted mechanism. The final reaction free energy is 4.7 ± 1.8 kcal/mol, which is slightly higher compared to the one estimated in the base-assisted route (2.6 ± 0.8 kcal/mol). According to the confidence intervals, the difference would not be statistically significant and therefore it could be safely attributed to minor factors such as insufficient sampling, PMF integration error and the different definitions of the *s* coordinate (which is path-dependent).

These results suggest that the substrate-assisted pathway is a less favorable mechanistic route compared to the base-assisted mechanism in the 2-Mg system, which is in agreement with previous results from QM/MM computational studies in CDK2[35,36] with one Mg^{2+} ion within the active site and in PKA with two metal cofactors.[40] The higher free energy barrier would be the result of a strained four-membered ring formed at the transition state (P_γ-$O_{2\gamma}$-$H_{\gamma(Thr)}$-$O_{\gamma(Thr)}$), a structural fact that imposes an extra energy penalty due to geometrical restrictions.[40] Here, QM/MM calculations in PKA have predicted potential energy barriers for the substrate-assisted mechanism that range from 27 to 34 kcal/mol considering different γ-phosphate oxygens as proton acceptors[40], results that would be in agreement with our estimation, though important methodological differences should be considered. On the other hand, the substrate-assisted mechanism was also studied using the AM1/d-PhoT Hamiltonian which also resembled an associative-like mechanism as the one described by the DFTB3 method and with a similar activation free energy barrier (29.4 ± 0.8 kcal/mol, see SI for a detailed description).

3.2 Phosphoryl transfer mechanism with one Mg^{2+} ion

3. 2. 1. Base-assisted mechanism

The phosphoryl transfer mechanism in CDK2 was also studied with only one Mg^{2+} ion within the active site. Initial classical MD simulations of the reactant state showed that the nucleophilic threonine residue tended to leave the active site, differently to what was observed in the 2-Mg system. This behavior was also

observed previously in MD simulations performed by the authors that published the crystal structure used in this study, where they proposed that the weak apparent affinity of the peptide substrate (K_M=120 μM at 150 mM KCl) could be the cause of this event,[6] though another possible cause could be related to deficiencies in the force field. Thus, we performed MD simulations adding a soft positional restraint (see SI) to the peptide substrate except for the threonine residue. With this, the threonine residue was restricted to the active site, but the hydroxyl group could still sample different conformations. MD simulations showed that formation of HBs between the $O_{\gamma(Thr)}$-$H_{\gamma(Thr)}$ group with γ-phosphate oxygens was favorable, especially with oxygen $O_{1\gamma}$, and also with Asp127 (Fig. S7). Water molecules fill the space where Mg1 was originally located, and the entrance of water molecules causes a partial opening of the Gly-rich loop, which in turns allows the entrance of more water molecules at the active site (see Fig. S8). The partial opening of the Gly-rich loop generates the breakage of several HBs between the backbone amides of residues Thr14, Tyr15 and Gly16 from the Gly-rich loop with β-phosphate oxygen atoms. The missing HBs are replaced by their counterparts but with water molecules, which can also provide charge stabilization on the negatively charged phosphate oxygens. The opening of the Gly-rich loop is expected since crystallographic structures of CDK2 with one Mg^{2+} cofactor show this motif in an open conformation,[32] and MD simulations have shown that the presence of only one Mg^{2+} ion in the active site induces the open conformation of this loop.[6]

After classical MD, QM/MM MD simulations were performed for 100 ps using QM/MM Hamiltonians but without any restraints. It was found that, at least at this time scale, the substrate threonine residue was stable in the active site. Here, it was observed that the $O_{\gamma(Thr)}$-$H_{\gamma(Thr)}$ group was mostly positioned to form HBs with the γ-phosphate oxygens, while HBs with Asp127 were hardly formed (Fig. S9). Thus, the initial reactant structure for the adaptive string calculations using both Hamiltonians features the hydroxyl group forming a HB with the phosphate oxygen $O_{1\gamma}$, with rather long $H_{\gamma(Thr)}$-$O_{\delta1(Asp127)}$ distances (Fig. 8A). On the other hand, the product conformation was also relaxed, and it shows a protonated Asp127 residue making a HB with the $O_{\gamma(Thr)}$ oxygen (Fig. 8E). The main change in

555 the active site is the new conformation that the transferred phosphoryl group
556 adopts in the product state, where it is seen that the plane formed by the three γ-
557 phosphate oxygens is now roughly perpendicular to the plane formed by the β-
558 phosphate oxygens, in a "down" conformation facing the bulk (see Fig. 8E). This
559 conformation is adopted since the $O_{1\gamma}$ atom is no longer interacting with the Mg1
560 ion and therefore the phosphate group is free to adopt a different pose in the active
561 site.

562

563 After observing that the base-assisted mechanism was preferred in the 2-Mg
564 system, we decided to only study this pathway in the 1-Mg system. Fig. 9 shows
565 the free energy profile with the evolution of the corresponding CVs (see Fig. S10
566 for string convergence) for the base-assisted mechanism in the 1-Mg system. In
567 this case, the same CVs used to study the base-assisted mechanism in the 2-Mg
568 system (steps 1 and 2) were used. Differently to the mechanism described
569 previously for the 2-Mg system, for the 1-Mg system only the first part of the base-
570 assisted mechanism (step 1, Fig. 2) was studied. The reason is that we were not
571 able to capture in our string simulations the complete base-assisted mechanism
572 with the final proton transfer from Asp127 to the $O_{2\gamma}$ atom of the phosphate group
573 (step 2). However, this does not alter our discussion since it is expected that the
574 last proton transfer, if exists, would not be the rate-limiting step.

575

576 As was previously stated, one Mg^{2+} ion in the active site preferentially stabilizes
577 HBs between the threonine's hydroxyl group with γ-phosphate oxygens, and
578 therefore, the first step during the mechanism is the gradual approach of this
579 hydroxyl group towards the oxygen $O_{\delta1(Asp127)}$ (Fig. 9B). This process is reflected in
580 the decrease of CVs 4 ($H_{\gamma(Thr)}$-$O_{\delta1(Asp127)}$) and 7 ($O_{\gamma(Thr)}$-$O_{\delta1(Asp127)}$) until *s* value of
581 5.27 (Fig. 8B and solid vertical line in Fig. 9). Also, in this first part of the
582 mechanism both the donor and the acceptor fragments begin to approach each
583 other (decrease in CVs 2 and 6) but without dissociation of the $O_{3\beta}$-P_γ bond, which
584 takes an approximate free energy cost of 6.2 kcal/mol. Once the $O_{\gamma(Thr)}$-$H_{\gamma(Thr)}$ bond
585 has been positioned to make a HB with Asp127, the $O_{3\beta}$-P_γ bond begins to break

and the P_γ-$O_{\gamma(Thr)}$ bond is further formed. This occurs until the transition state (TSe) is reached (Fig. 8C and dashed vertical line in Fig. 9), where CV1 and CV2 take average values of 2.35 and 2.64 Å, respectively. Thus, the transition state has a dissociative character of 95%, and therefore is not very different to the TSs (TS1a and TS2a) found for the base-assisted mechanism in the presence of two Mg^{2+} ions (94 and 93%, respectively). The associated free energy barrier to TSe amounts to 19.5 ± 0.6 kcal/mol, which is 2.9 kcal/mol higher compared to the free energy barrier obtained for the 2-Mg system at the DFTB3/ff99SB level. According to the activation free energies in both systems, these results corroborate the experimental observations that show that two Mg^{2+} ions are required for a more efficient phosphoryl transfer reaction.[6,14] However, considering that the difference is not too large, it is expected that the 1-Mg system may still be active. From TSe, the distance P_γ-$O_{\gamma(Thr)}$ (CV2) varies little, while the distance $O_{3\beta}$-P_γ (CV1) keeps increasing, generating structures with an even higher dissociative character. For instance, at s = 11.24, CV1 and CV2 take average values of 3.19 and 2.51 Å, respectively, giving a dissociative character of ≈ 99%, as it is also evidenced by the long $O_{3\beta}$-$O_{\gamma(Thr)}$ distance (CV6 = 5.35 Å). Fig. 8D shows a representative structure at this point in the reaction coordinate, where it is possible to see that this high dissociative character involves the conformational change previously mentioned in the transferred phosphoryl group (the "down" conformation). Subsequently, the proton transfer is carried out simultaneously with the complete formation of the P_γ-$O_{\gamma(Thr)}$ bond, without any additional energy barrier, but on the contrary, contributing to the lowering of the free energy.

An interesting point is the exergonic character of the reaction, with a reaction free energy of -8.2 kcal/mol, which is very different to the reaction free energy obtained for the 2-Mg system (2.6 kcal/mol). In the study of Smith *et al*.[35] in CDK2, where QM/MM free energy calculations were performed (at the B3LYP/ff99SB level), a negative reaction free energy was predicted (slightly lower than -10 kcal/mol), in agreement with our current estimation. It is also worth noting that we did not observe these highly dissociative structures and the conformational change in the transferred phosphoryl group in our previous QM/MM study in

CDK2 with one Mg^{2+} ion (PES exploration),[36] suggesting that incorporation of the protein environment in a flexible way (free energy simulations) seems to be an important aspect to take into account. On the other hand, calculations with the AM1/d-PhoT Hamiltonian predicted a similar mechanism to the one predicted for the 2-Mg system at that level of theory, but also with a higher free energy barrier (details in SI), correlating well with the results using the DFTB3 method and experimental findings. We would like to mention that there are other open questions not addressed in the present investigation, as it is the role of Lys129 in the reaction. In a previous study in our group[36], its role as a proton donor to the transferred phosphoryl group along the base-assisted mechanism was found to be viable in the presence of one Mg^{2+} ion. In the meantime, it is clear that residue Lys129 is well positioned in the active site to assist the phosphoryl transfer reaction and it helps to stabilize the negative charge on the γ-phosphoryl group at the transition and product state.

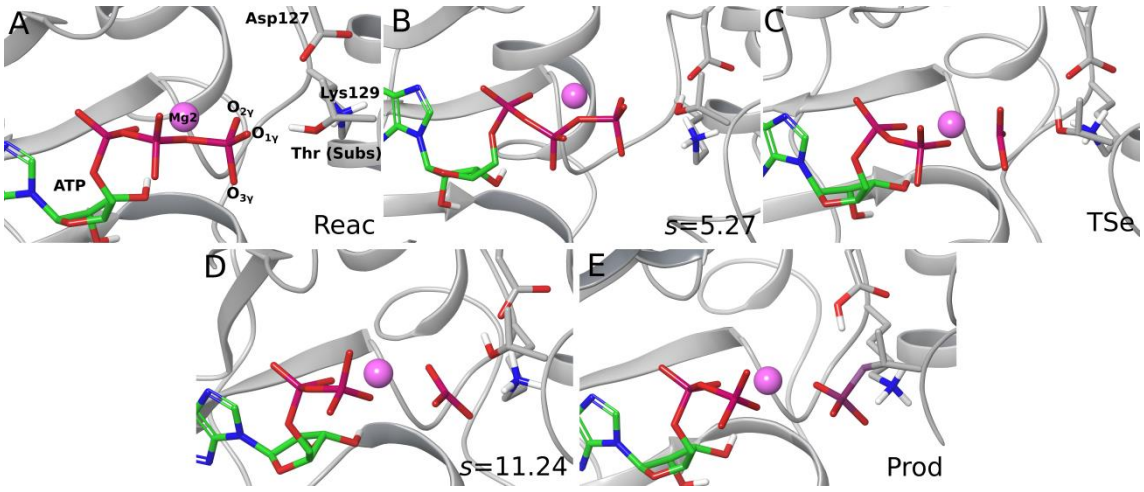

Figure 8. (A-E) Representative structures of reactants, products, transition state TSe and important points in the reaction's progression identified according to the free energy profile of Fig. 9. The residue Lys129 is also shown in the structures to highlight its role in the stabilization of the γ-phosphoryl group through electrostatic and hydrogen bonding interactions.

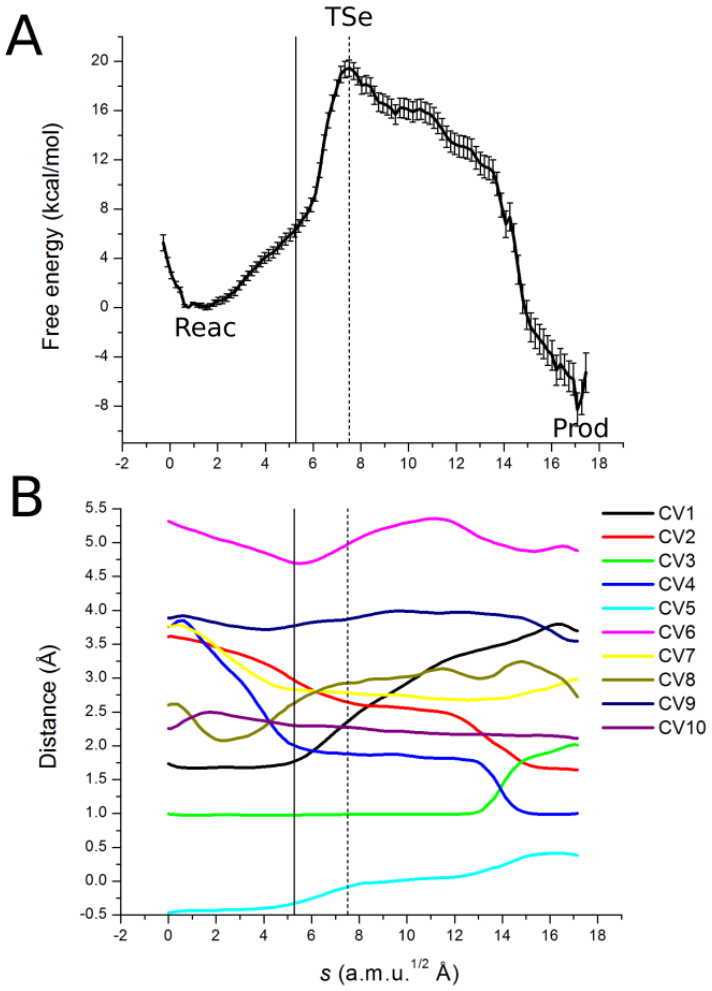

Figure 9. (A) Free energy profile for the base-assisted mechanism (step 1), with one Mg^{2+} ion in the active site, along the reaction coordinate *s* calculated at the DFTB3/ff99SB level. PMF calculated over 90 ps of sampling in each window. Error bars correspond to 95% confidence intervals. Solid vertical line represents the point on the reaction where the rotation of the threonine's hydroxyl group towards Asp127 has been completed. Dashed vertical line represents the position of the transition state TSe on the reaction coordinate. (B) Evolution of the CVs along the reaction coordinate *s*.

3.3 Enhanced repulsion in the 1-Mg system

In order to rationalize the effects of an additional Mg^{2+} ion within the active site of CDK2, Mulliken charges were analyzed for the paths defined in the base-assisted mechanism (the most probable one) for both 1-Mg and 2-Mg systems at the DFTB3/ff99SB level. It was found that in general both systems exhibit the same trends for the atoms involved in the phosphoryl transfer reaction (Fig. S11). These trends also agree with the results obtained in our previous study in CDK2 with one Mg^{2+} ion in the active site, where NPA (natural population analysis) charges were calculated.[36] However, we noticed that the charges on the γ-phosphoryl oxygen atoms and therefore on the γ-phosphoryl group were shifted to more negative values in the 1-Mg system. This suggests that in the case of the 1-Mg system, a larger repulsion should be felt by the reacting fragments, clearly affecting the free energy barrier. A more detailed analysis of Mulliken charges can be found in the SI.

In order to get deeper insights into the differences in free energy barriers between 1-Mg and 2-Mg systems, free energy contributions associated to each CV[72] were analyzed (Fig. S12). It is worth mentioning that these free energy contributions should not be considered as "bond energies", but rather as a way to detect the coordinates through which free energy can be released or introduced into the system. Here, it is observed that for the 2-Mg and 1-Mg systems, the initial increment in the free energy barrier is mostly associated with CV2, which describes the approach of $O_{\gamma(Thr)}$ to P_{γ}. This represents the electrostatic repulsion that must be overcome once both atoms begin to approach each other. When reaching the respective TSs, the total free energy contribution associated to CV2 is 17.4 and 9.4 kcal/mol for 1-Mg and 2-Mg systems, respectively (Fig. S12). Also, the contribution from CV6, that represents the donor-acceptor ($O_{3\beta}$-O_{γ}) distance, is higher in the 1-Mg system compared to the 2-Mg system. An additional contribution that increases the activation free energy in the 1-Mg system is due to CV7, coordinate that characterizes the approach of the $O_{\gamma(Thr)}$-$H_{\gamma(Thr)}$ group to Asp127 (see Fig. 9). Until the rotation of this hydroxyl group towards Asp127 has been completed (solid vertical line in Fig. S12B), the free energy increment associated to this CV is 2.6 kcal/mol. Thus, this analysis confirms that the greater repulsion experienced by the reacting fragments in the 1-Mg system and the

685 unfavorable conformation of the threonine's hydroxyl group are the main factors
686 that explain the less favorable catalytic activity. A more detailed analysis of CVs
687 contributions is given in the SI.

688

689 4. Discussion

690 During the study of the 2-Mg system at the DFTB3/ff99SB level, the base-assisted
691 mechanism was found to be the most favorable mechanistic route (16.6 ± 0.5
692 kcal/mol compared to 26.2 ± 1.3 kcal/mol for the substrate-assisted mechanism).
693 In this mechanism, Asp127 acts as a base activating the nucleophilic hydroxyl
694 group through a HB interaction and receiving the proton once the phosphoryl
695 transfer is almost completed. This late proton transfer reaction to Asp127 was also
696 detected in previous computational studies in CDK2 with one Mg^{2+} ion[35,36] and in
697 computational studies in PKA with two metal ions[40,41,48,49] to its homologous
698 residue (Asp166). We explored through the adaptive string method the complete
699 base-assisted mechanism, which involves, in a second step, a proton transfer from
700 Asp127 to one of the γ-phosphate oxygens ($O_{2\gamma}$ in this case), leaving the
701 transferred phosphoryl group protonated. QM/MM potential energy calculations
702 performed in the enzyme PKA at the B3LYP/CHARMM level of theory have
703 proposed this mechanism as the most favorable one.[40] With this, it was found that
704 the estimated free energy barrier for the base-assisted mechanism (16.6 kcal/mol)
705 agrees well with the experimental derived value of 15.3 kcal/mol.[24]

706

707 The phosphoryl transfer mechanism was also studied with one Mg^{2+} ion in the
708 active site. The calculated free energy barrier in the 1-Mg system (19.5 ± 0.6
709 kcal/mol) is ~3 kcal/mol higher compared to the activation energy in the 2-Mg
710 system. These free energy values are compatible with the experimental
711 observation that CDK2 already catalyzes the reaction with one Mg^{2+} ion but is more
712 efficient with two Mg^{2+} ions as cofactors.[6,14] An important point to notice is that
713 upon the absence of Mg1, the conformational equilibrium of the target threonine's
714 hydroxyl group between conformations that favor HBs with γ-phosphate oxygens

and Asp127 is altered. In this regard, a possible explanation is that the entrance of water molecules in the active site (Fig. S8) screen the interaction between the $O_{\gamma(Thr)}$-$H_{\gamma(Thr)}$ group and Asp127, imposing an extra energy penalty for the rotation of the threonine's hydroxyl group. Besides, it is expected that the more flexible coordination of the ATP molecule in the 1-Mg system may affect the interactions that the substrate hydroxyl group forms with Asp127.

Analysis of Mulliken charges and free energy contributions associated to each CV on the total free energy profile showed that an enhanced repulsion between the reacting fragments would be the main cause for the higher activation free energy in the 1-Mg system. The presence of Mg1 helps to stabilize the negative charge on the ATP molecule, and especially on the γ-phosphate group, reducing the electrostatic repulsion with the nucleophilic hydroxyl group and stabilizing the transition state. Upon the absence of Mg1, the phosphoryl transfer can still occur since the enhanced repulsion felt by the reacting fragments is somewhat compensated but the higher flexibility that the transferred phosphoryl group has, which is more free to accommodate in the active site, resulting in a more dissociative mechanism, but with a reduced efficiency. Finally, the presence of the second Mg^{2+} ion leads to a more rigidified active site that allows a "down" or closed conformation of the Gly-rich loop, expelling in this process water molecules from the active site (see Fig. S8), as it has also been observed in previous studies.[6] In general, water molecules follow the charge flow taking place during the chemical reaction but at the cost of a larger reorganization energy, which is then translated into a larger activation free energy. This concept has also been expressed as the importance of "not being in water for catalysis".[86]

With respect to the available experimental data, we would like to mention that it is difficult to assess if the kinetic parameter that was derived from experiments (k_3= 35 s^{-1})[24] was measured in the presence of one or two Mg^{2+} ions within the active site of CDK2. The crystal structure of the transition state mimic used in this study that was able to capture Mg1 in the active site came from crystals grown in 20 mM

of $MgCl_2$, which were then transferred and soaked in a solution of 10 mM of $MgCl_2$,[6] and therefore the exact concentration that allows to have the Mg1 site occupied is difficult to determine. However, it is highly probable that the concentration of $MgCl_2$ used in the kinetic experiments (10 mM) has been high enough to have the Mg1 site occupied. Titration experiments have estimated K_D for the Mg1 site to 5-7 mM for the ADP-Mg bound enzyme complex,[6] but one would expect a lower value for the ATP-Mg bound enzyme complex. Therefore, it is safe to assume that the concentration used in the kinetic experiments was high enough to occupy both metal binding sites. Besides, though in the last studies of CDK2[6,14] the microscopic rate constant corresponding to the chemical step was not estimated, our results confirm the experimental trends that show a strong increase in reaction velocity upon increasing Mg^{2+} concentration. Interestingly, similar experimental results have been found for CDK5,[7] with which CDK2 shares ~60% sequence similarity, where a second Mg^{2+} ion was found to be required for optimal catalysis.

In this context, these findings could have a direct implication in CDK function. Here, it has been proposed that the concentration of free Mg^{2+} during the cell cycle can vary[87] and misregulation of Mg^{2+} levels can have an effect in cell differentiation and proliferation.[88] This opens the possibility that CDK activity may be regulated by local fluctuations in Mg^{2+} concentration during the cell cycle.[6] This phenomenon has been recently explored in kinases that are involved T-cell activation,[89] where it was found that the presence of a second Mg^{2+} ion (Mg1) in the active site fulfills a regulatory function of the kinase activity. With this, it was proposed that millimolar changes in free basal Mg^{2+} play a crucial role in kinase regulation and function, changing in this way the classical paradigm of how kinases are regulated.[89]

Finally, with respect to the level of the calculations, some clarifying sentences could be helpful. The DFTB3 method has been extensively used in recent years for the discrimination of reaction mechanisms in phosphoryl transfer reactions,[47,64–66] and in particular, it was recently successfully used in QM/MM simulations for

evaluating the influence of a third Mg^{2+} ion on the nucleotide addition by DNA polymerase,[90] showing the method as a valuable tool to discriminate among reaction mechanisms at a reasonable computational cost. However, care should be taken since the method is only a semiempirical approach and therefore only allows for a semi-quantitative analysis. Despite this, studies in previous phosphoryl transfer related reactions have shown that the method is semi-quantitatively consistent with calculations using the B3LYP DFT functional, though in general the exothermicity of phosphoryl transfer reactions is overestimated.[66,90] In this context, we expect errors arising from the level of theory, and therefore we do not consider the absolute values in free energies as being quantitatively conclusive. On the other hand, we expect these errors to be systematic along the calculations, and upon comparison among mechanisms, some error cancelation should take place, and hence the observed trends should be reliable. As was discussed in the manuscript, interestingly, the results obtained with the DFTB3 method for the description of the base-assisted mechanism in the 2-Mg system qualitatively agree with the phosphoryl transfer mechanism proposed for the enzyme PKA,[40] which was calculated using PESs at the B3LYP/CHARMM level, giving indirect evidence of the reliability of our calculations and a more unified view on which is the most probable reaction mechanism in protein kinases.

5. Conclusions

In the present computational study, the phosphoryl transfer reaction in CDK2 was revisited using a more recent crystallographic structure as a model that contained two Mg^{2+} ions at the active site, what allowed us to study the influence of the second magnesium ion (Mg1) in the reaction mechanism. Furthermore, the different proposed mechanisms, namely base-assisted and substrate-assisted pathways, were examined in detail. QM/MM simulations allowed the calculation of activation free energies in order to discriminate the most probable mechanistic option. For the 2-Mg system, the base-assisted mechanism, where Asp127 acts firstly as a catalytic base extracting the nucleophilic hydroxyl's proton and later as a catalytic acid protonating the transferred phosphoryl group, was found to be the

most probable route. At the DFTB3/ff99SB level of theory, the free energy barrier was estimated to 16.6 ± 0.5 kcal/mol, and the mechanism was characterized with a high dissociative character, in agreement with experimental results and other previous computational studies. On the other hand, the substrate-assisted mechanism at the same level of theory was characterized as concerted, with a lower dissociative character, and with a higher free energy barrier (26.2 ± 1.3 kcal/mol), making it a less probable mechanistic option, in agreement with previous computational studies in CDK2 with one Mg^{2+} ion in the active site[35,36] and in the enzyme PKA with two metal cofactors.[40]

The study of the phosphoryl transfer reaction with only one Mg^{2+} ion at the active site showed that the absence of one of the ions generates a higher free energy barrier in the base-assisted mechanism (19.5 ± 0.6 kcal/mol at the DFTB3/ff99SB level) compared to the 2-Mg system. Analysis of the free energy profile decompositions, as well as atomic charges, allowed us to identify that an enhanced repulsion between the reacting fragments is the main cause for the difference in the reaction barriers. Besides, the conformational equilibrium of the nucleophilic threonine's hydroxyl group is altered in the 1-Mg system, where HBs with Asp127 are not energetically favored, and therefore an extra energy penalty must be paid to reach a reactive conformation. Finally, a Mg-dependent conformational change of the Gly-rich group seems to be important to improve the catalytic properties of the active site when two Mg^{2+} ions are present. Altogether, the results presented in this study corroborate experimental evidence of a more efficient phosphoryl transfer reaction with two Mg^{2+} ions in the active site of CDK2[6,14] and provide molecular insights explaining this effect. In general, our results are in agreement with previous observations that two Mg^{2+} ions are needed in the active site of CDK2 and other protein kinases to satisfy the so-called charge balance hypothesis (CBH),[91,92] which states that local charge balance is the most important effect for the stabilization of the TS in phosphoryl transfer reactions. These results are expected to broaden the understanding of how Mg^{2+} ions regulate kinase activity, and it is yet to understand how other kinases may work more efficiently with only

one Mg^{2+} ion at the active site or if a "two metal catalysis", as proposed here, is the predominant mechanism in kinases.

Supporting Information

Acknowledgements

RR acknowledges support from a doctoral fellowship CONICYT-PCHA/Folio 21130949. IT acknowledges support by the Spanish Ministerio de Economía y Competitividad and FEDER funds (project PGC2018-094852-B-C22). RR and JA-M thank the financial support from project FONDECYT Nº 1181253.

References

(1) Kamerlin, S. C. L.; Sharma, P. K.; Prasad, R. B.; Warshel, A. Why Nature Really Chose Phosphate. *Q Rev Biophys* **2013**, *46*, 1–132.

(2) Adams, J. A. Kinetic and Catalytic Mechanisms of Protein Kinases. *Chem. Rev.* **2001**, *101* (8), 2271–2290. https://doi.org/10.1021/cr000230w.

(3) Endicott, J. A.; Noble, M. E. M.; Johnson, L. N. The Structural Basis for Control of Eukaryotic Protein Kinases. *Annu. Rev. Biochem.* **2012**, *81*, 587–613. https://doi.org/10.1146/annurev-biochem-052410-090317.

(4) Russo, A. A.; Jeffrey, P. D.; Pavletich, N. P. Structural Basis of Cyclin-Dependent Kinase Activation by Phosphorylation. *Nat. Struct. Biol.* **1996**, *3* (8), 696. https://doi.org/10.1038/nsb0896-696.

(5) Jeffrey, P. D.; Russo, A. A.; Polyak, K.; Gibbs, E.; Hurwitz, J.; Massagué, J.; Pavletich, N. P. Mechanism of CDK Activation Revealed by the Structure of a CyclinA-CDK2 Complex. *Nature* **1995**, *376* (6538), 313. https://doi.org/10.1038/376313a0.

(6) Bao, Z. Q.; Jacobsen, D. M.; Young, M. A. Briefly Bound to Activate: Transient Binding of a Second Catalytic Magnesium Activates the Structure and Dynamics of CDK2 Kinase for Catalysis. *Struct. Lond. Engl. 1993* **2011**, *19* (5), 675–690. https://doi.org/10.1016/j.str.2011.02.016.

(7) Liu, M.; Girma, E.; Glicksman, M. A.; Stein, R. L. Kinetic Mechanistic Studies of Cdk5/P25-Catalyzed H1P Phosphorylation: Metal Effect and Solvent Kinetic Isotope Effect. *Biochemistry* **2010**, *49* (23), 4921–4929. https://doi.org/10.1021/bi100244j.

(8) Waas, W. F.; Dalby, K. N. Physiological Concentrations of Divalent Magnesium Ion Activate the Serine/Threonine Specific Protein Kinase ERK2. *Biochemistry* **2003**, *42* (10), 2960–2970. https://doi.org/10.1021/bi027171w.

(9) Sun, G.; Budde, R. J. A. Requirement for an Additional Divalent Metal Cation To Activate Protein Tyrosine Kinases. *Biochemistry* **1997**, *36* (8), 2139–2146. https://doi.org/10.1021/bi962291n.

(10) Adams, J. A.; Taylor, S. S. Divalent Metal Ions Influence Catalysis and Active-Site Accessibility in the CAMP-Dependent Protein Kinase. *Protein Sci. Publ. Protein Soc.* **1993**, *2* (12), 2177–2186. https://doi.org/10.1002/pro.5560021217.

(11) Cook, P. F.; Neville, M. E.; Vrana, K. E.; Hartl, F. T.; Roskoski, R. Adenosine Cyclic 3',5'-Monophosphate Dependent Protein Kinase: Kinetic Mechanism for the Bovine Skeletal Muscle Catalytic Subunit. *Biochemistry* **1982**, *21* (23), 5794–5799. https://doi.org/10.1021/bi00266a011.

(12) Shaffer, J.; Adams, J. A. An ATP-Linked Structural Change in Protein Kinase A Precedes Phosphoryl Transfer under Physiological Magnesium Concentrations. *Biochemistry* **1999**, *38* (17), 5572–5581. https://doi.org/10.1021/bi982768q.

(13) Cook, A.; Lowe, E. D.; Chrysina, E. D.; Skamnaki, V. T.; Oikonomakos, N. G.; Johnson, L. N. Structural Studies on Phospho-CDK2/Cyclin A Bound to Nitrate, a Transition State Analogue: Implications for the Protein Kinase Mechanism. *Biochemistry* **2002**, *41* (23), 7301–7311.

(14) Jacobsen, D. M.; Bao, Z.-Q.; O'Brien, P.; Brooks, C. L.; Young, M. A. Price To Be Paid for Two-Metal Catalysis: Magnesium Ions That Accelerate Chemistry Unavoidably Limit Product Release from a Protein Kinase. *J. Am. Chem. Soc.* **2012**, *134* (37), 15357–15370. https://doi.org/10.1021/ja304419t.

(15) Morgan, D. O. Principles of CDK Regulation. *Nature* **1995**, *374* (6518), 131–134. https://doi.org/10.1038/374131a0.

(16) Desai, D.; Gu, Y.; Morgan, D. O. Activation of Human Cyclin-Dependent Kinases in Vitro. *Mol. Biol. Cell* **1992**, *3* (5), 571–582.

(17) Connell-Crowley, L.; Solomon, M. J.; Wei, N.; Harper, J. W. Phosphorylation Independent Activation of Human Cyclin-Dependent Kinase 2 by Cyclin A in Vitro. *Mol. Biol. Cell* **1993**, *4* (1), 79–92.

(18) Bloom, J.; Cross, F. R. Multiple Levels of Cyclin Specificity in Cell-Cycle Control. *Nat. Rev. Mol. Cell Biol.* **2007**, *8* (2), 149–160. https://doi.org/10.1038/nrm2105.

(19) Gould, K. L.; Moreno, S.; Owen, D. J.; Sazer, S.; Nurse, P. Phosphorylation at Thr167 Is Required for Schizosaccharomyces Pombe P34cdc2 Function. *EMBO J.* **1991**, *10* (11), 3297–3309.

(20) Krek, W.; Nigg, E. A. Cell Cycle Regulation of Vertebrate P34cdc2 Activity: Identification of Thr161 as an Essential in Vivo Phosphorylation Site. *New Biol.* **1992**, *4* (4), 323–329.

(21) Gu, Y.; Rosenblatt, J.; Morgan, D. O. Cell Cycle Regulation of CDK2 Activity by Phosphorylation of Thr160 and Tyr15. *EMBO J.* **1992**, *11* (11), 3995–4005.

(22) Solomon, M. J. Activation of the Various Cyclin/Cdc2 Protein Kinases. *Curr. Opin. Cell Biol.* **1993**, *5* (2), 180–186. https://doi.org/10.1016/0955-0674(93)90100-5.

(23) Ducommun, B.; Brambilla, P.; Félix, M. A.; Franza, B. R.; Karsenti, E.; Draetta, G. Cdc2 Phosphorylation Is Required for Its Interaction with Cyclin. *EMBO J.* **1991**, *10* (11), 3311–3319.

(24) Stevenson, L. M.; Deal, M. S.; Hagopian, J. C.; Lew, J. Activation Mechanism of CDK2: Role of Cyclin Binding versus Phosphorylation. *Biochemistry* **2002**, *41* (26), 8528–8534. https://doi.org/10.1021/bi025812h.

(25) Lim, S.; Kaldis, P. Cdks, Cyclins and CKIs: Roles beyond Cell Cycle Regulation. *Dev. Camb. Engl.* **2013**, *140* (15), 3079–3093. https://doi.org/10.1242/dev.091744.

(26) Wood, D. J.; Endicott, J. A. Structural Insights into the Functional Diversity of the CDK-Cyclin Family. *Open Biol.* **2018**, *8* (9). https://doi.org/10.1098/rsob.180112.

(27) Lapenna, S.; Giordano, A. Cell Cycle Kinases as Therapeutic Targets for Cancer. *Nat. Rev. Drug Discov.* **2009**, *8* (7), 547–566. https://doi.org/10.1038/nrd2907.

(28) Malumbres, M.; Pevarello, P.; Barbacid, M.; Bischoff, J. R. CDK Inhibitors in Cancer Therapy: What Is Next? *Trends Pharmacol. Sci.* **2008**, *29* (1), 16–21. https://doi.org/10.1016/j.tips.2007.10.012.

(29) McInnes, C. Progress in the Evaluation of CDK Inhibitors as Anti-Tumor Agents. *Drug Discov. Today* **2008**, *13* (19–20), 875–881. https://doi.org/10.1016/j.drudis.2008.06.012.

(30) Asghar, U.; Witkiewicz, A. K.; Turner, N. C.; Knudsen, E. S. The History and Future of Targeting Cyclin-Dependent Kinases in Cancer Therapy. *Nat. Rev. Drug Discov.* **2015**, *14* (2), 130–146. https://doi.org/10.1038/nrd4504.

(31) Storer, A. C.; Cornish-Bowden, A. Kinetics of Rat Liver Glucokinase. Co-Operative Interactions with Glucose at Physiologically Significant Concentrations. *Biochem. J.* **1976**, *159* (1), 7–14.

(32) Brown, N. R.; Noble, M. E.; Endicott, J. A.; Johnson, L. N. The Structural Basis for Specificity of Substrate and Recruitment Peptides for Cyclin-Dependent Kinases. *Nat. Cell Biol.* **1999**, *1* (7), 438–443. https://doi.org/10.1038/15674.

(33) Cavalli, A.; Vivo, M. D.; Recanatini, M. Density Functional Study of the Enzymatic Reaction Catalyzed by a Cyclin-Dependent Kinase. *Chem. Commun.* **2003**, *0* (11), 1308–1309. https://doi.org/10.1039/B212618D.

(34) De Vivo, M.; Cavalli, A.; Carloni, P.; Recanatini, M. Computational Study of the Phosphoryl Transfer Catalyzed by a Cyclin-Dependent Kinase. *Chem. – Eur. J.* **2007**, *13* (30), 8437–8444. https://doi.org/10.1002/chem.200700044.

(35) Smith, G. K.; Ke, Z.; Guo, H.; Hengge, A. C. Insights into the Phosphoryl Transfer Mechanism of Cyclin-Dependent Protein Kinases from Ab Initio QM/MM Free-Energy Studies. *J. Phys. Chem. B* **2011**, *115* (46), 13713–13722. https://doi.org/10.1021/jp207532s.

(36) Recabarren, R.; Osorio, E. H.; Caballero, J.; Tuñón, I.; Alzate-Morales, J. H. Mechanistic Insights into the Phosphoryl Transfer Reaction in Cyclin-Dependent Kinase 2: A QM/MM Study. *PLOS ONE* **2019**, *14* (9), e0215793. https://doi.org/10.1371/journal.pone.0215793.

(37) Madhusudan, null; Akamine, P.; Xuong, N.-H.; Taylor, S. S. Crystal Structure of a Transition State Mimic of the Catalytic Subunit of CAMP-Dependent Protein Kinase. *Nat. Struct. Biol.* **2002**, *9* (4), 273–277. https://doi.org/10.1038/nsb780.

(38) Bastidas, A. C.; Deal, M. S.; Steichen, J. M.; Guo, Y.; Wu, J.; Taylor, S. S. Phosphoryl Transfer by Protein Kinase A Is Captured in a Crystal Lattice. *J. Am. Chem. Soc.* **2013**, *135* (12), 4788–4798. https://doi.org/10.1021/ja312237q.

(39) Lassila, J. K.; Zalatan, J. G.; Herschlag, D. Biological Phosphoryl-Transfer Reactions: Understanding Mechanism and Catalysis. *Annu. Rev. Biochem.* **2011**, *80*, 669–702. https://doi.org/10.1146/annurev-biochem-060409-092741.

(40) Pérez-Gallegos, A.; Garcia-Viloca, M.; González-Lafont, À.; Lluch, J. M. SP20 Phosphorylation Reaction Catalyzed by Protein Kinase A: QM/MM Calculations Based on Recently Determined Crystallographic Structures. *ACS Catal.* **2015**, *5* (8), 4897–4912. https://doi.org/10.1021/acscatal.5b01064.

(41) Valiev, M.; Yang, J.; Adams, J. A.; Taylor, S. S.; Weare, J. H. Phosphorylation Reaction in CAPK Protein Kinase-Free Energy Quantum Mechanical/Molecular Mechanics Simulations. *J. Phys. Chem. B* **2007**, *111* (47), 13455–13464. https://doi.org/10.1021/jp074853q.

(42) Pérez-Gallegos, A.; Garcia-Viloca, M.; González-Lafont, À.; Lluch, J. M. A QM/MM Study of Kemptide Phosphorylation Catalyzed by Protein Kinase A. The Role of Asp166 as a General Acid/Base Catalyst. *Phys. Chem. Chem. Phys. PCCP* **2015**, *17* (5), 3497–3511. https://doi.org/10.1039/c4cp03579h.

(43) Gerlits, O.; Tian, J.; Das, A.; Langan, P.; Heller, W. T.; Kovalevsky, A. Phosphoryl Transfer Reaction Snapshots in Crystals: Insights into the Mechanism of Protein Kinase A

977 Catalytic Subunit. *J. Biol. Chem.* **2015**, *290* (25), 15538–15548.
978 https://doi.org/10.1074/jbc.M115.643213.
979 (44) Alkherraz, A.; Kamerlin, S. C. L.; Feng, G.; Sheikh, Q. I.; Warshel, A.; Williams, N. H.
980 Phosphate Ester Analogues as Probes for Understanding Enzyme Catalysed Phosphoryl
981 Transfer. *Faraday Discuss.* **2010**, *145* (0), 281–299. https://doi.org/10.1039/B908398G.
982 (45) Duarte, F.; Åqvist, J.; Williams, N. H.; Kamerlin, S. C. L. Resolving Apparent Conflicts
983 between Theoretical and Experimental Models of Phosphate Monoester Hydrolysis. *J.*
984 *Am. Chem. Soc.* **2015**, *137* (3), 1081–1093. https://doi.org/10.1021/ja5082712.
985 (46) Petrović, D.; Szeler, K.; Kamerlin, S. C. L. Challenges and Advances in the Computational
986 Modeling of Biological Phosphate Hydrolysis. *Chem. Commun.* **2018**, *54* (25), 3077–
987 3089. https://doi.org/10.1039/C7CC09504J.
988 (47) Roston, D.; Lu, X.; Fang, D.; Demapan, D.; Cui, Q. Analysis of Phosphoryl-Transfer
989 Enzymes with QM/MM Free Energy Simulations. *Methods Enzymol.* **2018**, *607*, 53–90.
990 https://doi.org/10.1016/bs.mie.2018.05.005.
991 (48) Cheng, Y.; Zhang, Y.; McCammon, J. A. How Does the CAMP-Dependent Protein Kinase
992 Catalyze the Phosphorylation Reaction: An Ab Initio QM/MM Study. *J. Am. Chem. Soc.*
993 **2005**, *127* (5), 1553–1562. https://doi.org/10.1021/ja0464084.
994 (49) Díaz, N.; Field, M. J. Insights into the Phosphoryl-Transfer Mechanism of CAMP-
995 Dependent Protein Kinase from Quantum Chemical Calculations and Molecular
996 Dynamics Simulations. *J. Am. Chem. Soc.* **2004**, *126* (2), 529–542.
997 https://doi.org/10.1021/ja037277u.
998 (50) Murillo-López, J.; Zinovjev, K.; Pereira, H.; Caniuguir, A.; Garratt, R.; Babul, J.;
999 Recabarren, R.; Alzate-Morales, J.; Caballero, J.; Tuñón, I.; Cabrera, R. Studying the
1000 Phosphoryl Transfer Mechanism of the E. Coli Phosphofructokinase-2: From X-Ray
1001 Structure to Quantum Mechanics/Molecular Mechanics Simulations. *Chem. Sci.* **2019**,
1002 *10* (10), 2882–2892. https://doi.org/10.1039/C9SC00094A.
1003 (51) Ojeda-May, P.; Li, Y.; Ovchinnikov, V.; Nam, K. Role of Protein Dynamics in Allosteric
1004 Control of the Catalytic Phosphoryl Transfer of Insulin Receptor Kinase. *J. Am. Chem.*
1005 *Soc.* **2015**, *137* (39), 12454–12457. https://doi.org/10.1021/jacs.5b07996.
1006 (52) Bordes, I.; Castillo, R.; Moliner, V. Theoretical Study of the Phosphoryl Transfer Reaction
1007 from ATP to Dha Catalyzed by DhaK from Escherichia Coli. *J. Phys. Chem. B* **2017**, *121*
1008 (38), 8878–8892. https://doi.org/10.1021/acs.jpcb.7b04862.
1009 (53) Bordes, I.; García-Junceda, E.; Sánchez-Moreno, I.; Castillo, R.; Moliner, V.
1010 Computational Study of the Phosphoryl Donor Activity of Dihydroxyacetone Kinase from
1011 ATP to Inorganic Polyphosphate. *Int. J. Quantum Chem.* **2018**, *118* (9), e25520.
1012 https://doi.org/10.1002/qua.25520.
1013 (54) Szarek, P.; Dyguda-Kazimierowicz, E.; Tachibana, A.; Sokalski, W. A. Physical Nature of
1014 Intermolecular Interactions within CAMP-Dependent Protein Kinase Active Site:
1015 Differential Transition State Stabilization in Phosphoryl Transfer Reaction. *J. Phys. Chem.*
1016 *B* **2008**, *112* (37), 11819–11826. https://doi.org/10.1021/jp8040633.
1017 (55) Dyguda-Kazimierowicz, E.; Sokalski, W. A.; Leszczyński, J. Non-Empirical Study of the
1018 Phosphorylation Reaction Catalyzed by 4-Methyl-5-Beta-Hydroxyethylthiazole Kinase:
1019 Relevance of the Theory of Intermolecular Interactions. *J. Mol. Model.* **2007**, *13* (6–7),
1020 839–849. https://doi.org/10.1007/s00894-007-0192-9.
1021 (56) Li, Q.; Zheng, J.; Tan, H.; Li, X.; Chen, G.; Jia, Z. Unique Kinase Catalytic Mechanism of
1022 AceK with a Single Magnesium Ion. *PLOS ONE* **2013**, *8* (8), e72048.
1023 https://doi.org/10.1371/journal.pone.0072048.
1024 (57) Singh, U. C.; Kollman, P. A. A Combined Ab Initio Quantum Mechanical and Molecular
1025 Mechanical Method for Carrying out Simulations on Complex Molecular Systems:
1026 Applications to the CH3Cl + Cl− Exchange Reaction and Gas Phase Protonation of
1027 Polyethers. *J. Comput. Chem.* **1986**, *7* (6), 718–730.
1028 https://doi.org/10.1002/jcc.540070604.

(58) Field, M. J.; Bash, P. A.; Karplus, M. A Combined Quantum Mechanical and Molecular Mechanical Potential for Molecular Dynamics Simulations. *J. Comput. Chem.* **1990**, *11* (6), 700–733. https://doi.org/10.1002/jcc.540110605.

(59) Elstner, M.; Porezag, D.; Jungnickel, G.; Elsner, J.; Haugk, M.; Frauenheim, Th.; Suhai, S.; Seifert, G. Self-Consistent-Charge Density-Functional Tight-Binding Method for Simulations of Complex Materials Properties. *Phys. Rev. B* **1998**, *58* (11), 7260–7268. https://doi.org/10.1103/PhysRevB.58.7260.

(60) Gaus, M.; Cui, Q.; Elstner, M. DFTB3: Extension of the Self-Consistent-Charge Density-Functional Tight-Binding Method (SCC-DFTB). *J. Chem. Theory Comput.* **2011**, *7* (4), 931–948. https://doi.org/10.1021/ct100684s.

(61) Gaus, M.; Lu, X.; Elstner, M.; Cui, Q. Parameterization of DFTB3/3OB for Sulfur and Phosphorus for Chemical and Biological Applications. *J. Chem. Theory Comput.* **2014**, *10* (4), 1518–1537. https://doi.org/10.1021/ct401002w.

(62) Lu, X.; Gaus, M.; Elstner, M.; Cui, Q. Parametrization of DFTB3/3OB for Magnesium and Zinc for Chemical and Biological Applications. *J. Phys. Chem. B* **2015**, *119* (3), 1062–1082. https://doi.org/10.1021/jp506557r.

(63) Nam, K.; Cui, Q.; Gao, J.; York, D. M. Specific Reaction Parametrization of the AM1/d Hamiltonian for Phosphoryl Transfer Reactions: H, O, and P Atoms. *J. Chem. Theory Comput.* **2007**, *3* (2), 486–504. https://doi.org/10.1021/ct6002466.

(64) Roston, D.; Demapan, D.; Cui, Q. Leaving Group Ability Observably Affects Transition State Structure in a Single Enzyme Active Site. *J. Am. Chem. Soc.* **2016**, *138* (23), 7386–7394. https://doi.org/10.1021/jacs.6b03156.

(65) Roston, D.; Cui, Q. Substrate and Transition State Binding in Alkaline Phosphatase Analyzed by Computation of Oxygen Isotope Effects. *J. Am. Chem. Soc.* **2016**, *138* (36), 11946–11957. https://doi.org/10.1021/jacs.6b07347.

(66) Lu, X.; Ovchinnikov, V.; Demapan, D.; Roston, D.; Cui, Q. Regulation and Plasticity of Catalysis in Enzymes: Insights from Analysis of Mechanochemical Coupling in Myosin. *Biochemistry* **2017**, *56* (10), 1482–1497. https://doi.org/10.1021/acs.biochem.7b00016.

(67) López-Canut, V.; Martí, S.; Bertrán, J.; Moliner, V.; Tuñón, I. Theoretical Modeling of the Reaction Mechanism of Phosphate Monoester Hydrolysis in Alkaline Phosphatase. *J. Phys. Chem. B* **2009**, *113* (22), 7816–7824. https://doi.org/10.1021/jp901444g.

(68) López-Canut, V.; Roca, M.; Bertrán, J.; Moliner, V.; Tuñón, I. Theoretical Study of Phosphodiester Hydrolysis in Nucleotide Pyrophosphatase/Phosphodiesterase. Environmental Effects on the Reaction Mechanism. *J. Am. Chem. Soc.* **2010**, *132* (20), 6955–6963. https://doi.org/10.1021/ja908391v.

(69) López-Canut, V.; Roca, M.; Bertrán, J.; Moliner, V.; Tuñón, I. Promiscuity in Alkaline Phosphatase Superfamily. Unraveling Evolution through Molecular Simulations. *J. Am. Chem. Soc.* **2011**, *133* (31), 12050–12062. https://doi.org/10.1021/ja2017575.

(70) D.A. Case, D.S. Cerutti, T.E. Cheatham, III, T.A. Darden, R.E. Duke, T.J. Giese, H. Gohlke, A.W. Goetz, D. Greene, N. Homeyer, S. Izadi, A. Kovalenko, T.S. Lee, S. LeGrand, P. Li, C. Lin, J. Liu, T. Luchko, R. Luo, D. Mermelstein, K.M. Merz, G. Monard, H. Nguyen, I. Omelyan, A. Onufriev, F. Pan, R. Qi, D.R. Roe, A. Roitberg, C. Sagui, C.L. Simmerling, W.M. Botello-Smith, J. Swails, R.C. Walker, J. Wang, R.M. Wolf, X. Wu, L. Xiao, D.M. York and P.A. Kollman (2017), AMBER 2017, University of California, San Francisco.

(71) Maragliano, L.; Vanden-Eijnden, E. On-the-Fly String Method for Minimum Free Energy Paths Calculation. *Chem. Phys. Lett.* **2007**, *446* (1), 182–190. https://doi.org/10.1016/j.cplett.2007.08.017.

(72) Zinovjev, K.; Tuñón, I. Adaptive Finite Temperature String Method in Collective Variables. *J. Phys. Chem. A* **2017**, *121* (51), 9764–9772. https://doi.org/10.1021/acs.jpca.7b10842.

(73) Maragliano, L.; Fischer, A.; Vanden-Eijnden, E.; Ciccotti, G. String Method in Collective Variables: Minimum Free Energy Paths and Isocommittor Surfaces. *J. Chem. Phys.* **2006**, *125* (2), 24106. https://doi.org/10.1063/1.2212942.
(74) Zinovjev, K.; Tuñón, I. Reaction Coordinates and Transition States in Enzymatic Catalysis. *Wiley Interdiscip. Rev. Comput. Mol. Sci.* **2018**, *8* (1), e1329. https://doi.org/10.1002/wcms.1329.
(75) Zinovjev, K.; Ruiz-Pernía, J. J.; Tuñón, I. Toward an Automatic Determination of Enzymatic Reaction Mechanisms and Their Activation Free Energies. *J. Chem. Theory Comput.* **2013**, *9* (8), 3740–3749. https://doi.org/10.1021/ct400153r.
(76) Zinovjev, K.; Tuñón, I. Exploring Chemical Reactivity of Complex Systems with Path-Based Coordinates: Role of the Distance Metric. *J. Comput. Chem.* **2014**, *35* (23), 1672–1681. https://doi.org/10.1002/jcc.23673.
(77) Kästner, J. Umbrella Sampling. *Wiley Interdiscip. Rev. Comput. Mol. Sci.* **2011**, *1* (6), 932–942. https://doi.org/10.1002/wcms.66.
(78) Sugita, Y.; Kitao, A.; Okamoto, Y. Multidimensional Replica-Exchange Method for Free-Energy Calculations. *J. Chem. Phys.* **2000**, *113* (15), 6042–6051. https://doi.org/10.1063/1.1308516.
(79) Manna, R. N.; Zinovjev, K.; Tuñón, I.; Dybala-Defratyka, A. Dehydrochlorination of Hexachlorocyclohexanes Catalyzed by the LinA Dehydrohalogenase. A QM/MM Study. *J. Phys. Chem. B* **2015**, *119* (49), 15100–15109. https://doi.org/10.1021/acs.jpcb.5b07538.
(80) Aranda, J.; Zinovjev, K.; Roca, M.; Tuñón, I. Dynamics and Reactivity in Thermus Aquaticus N6-Adenine Methyltransferase. *J. Am. Chem. Soc.* **2014**, *136* (46), 16227–16239. https://doi.org/10.1021/ja5077124.
(81) Aranda, J.; Zinovjev, K.; Świderek, K.; Roca, M.; Tuñón, I. Unraveling the Reaction Mechanism of Enzymatic C5-Cytosine Methylation of DNA. A Combined Molecular Dynamics and QM/MM Study of Wild Type and Gln119 Variant. *ACS Catal.* **2016**, *6* (5), 3262–3276. https://doi.org/10.1021/acscatal.6b00394.
(82) Saez, D. A.; Zinovjev, K.; Tuñón, I.; Vöhringer-Martinez, E. Catalytic Reaction Mechanism in Native and Mutant Catechol-O-Methyltransferase from the Adaptive String Method and Mean Reaction Force Analysis. *J. Phys. Chem. B* **2018**, *122* (38), 8861–8871. https://doi.org/10.1021/acs.jpcb.8b07339.
(83) Stoffel, G. M. M.; Saez, D. A.; DeMirci, H.; Vögeli, B.; Rao, Y.; Zarzycki, J.; Yoshikuni, Y.; Wakatsuki, S.; Vöhringer-Martinez, E.; Erb, T. J. Four Amino Acids Define the CO2 Binding Pocket of Enoyl-CoA Carboxylases/Reductases. *Proc. Natl. Acad. Sci.* **2019**, *116* (28), 13964–13969. https://doi.org/10.1073/pnas.1901471116.
(84) Roca, M.; Navas-Yuste, S.; Zinovjev, K.; López-Estepa, M.; Gómez, S.; Fernández, F. J.; Vega, M. C.; Tuñón, I. Elucidating the Catalytic Reaction Mechanism of Orotate Phosphoribosyltransferase by Means of X-Ray Crystallography and Computational Simulations. *ACS Catal.* **2020**, *10* (3), 1871–1885. https://doi.org/10.1021/acscatal.9b05294.
(85) Mildvan, A. S. Mechanisms of Signaling and Related Enzymes. *Proteins* **1997**, *29* (4), 401–416.
(86) Richard, J. P.; Amyes, T. L.; Goryanova, B.; Zhai, X. Enzyme Architecture: On the Importance of Being in a Protein Cage. *Curr. Opin. Chem. Biol.* **2014**, *21*, 1–10. https://doi.org/10.1016/j.cbpa.2014.03.001.
(87) Walker, G. M. Magnesium and Cell Cycle Control: An Update. *Magnesium* **1986**, *5* (1), 9–23.
(88) Wolf, F. I.; Cittadini, A. Magnesium in Cell Proliferation and Differentiation. *Front. Biosci. J. Virtual Libr.* **1999**, *4*, D607-617. https://doi.org/10.2741/wolf.
(89) Kanellopoulou, C.; George, A. B.; Masutani, E.; Cannons, J. L.; Ravell, J. C.; Yamamoto, T. N.; Smelkinson, M. G.; Jiang, P. D.; Matsuda-Lennikov, M.; Reilley, J.; Handon, R.; Lee, P.-H.; Miller, J. R.; Restifo, N. P.; Zheng, L.; Schwartzberg, P. L.; Young, M.; Lenardo, M. J.

Mg2+ Regulation of Kinase Signaling and Immune Function. *J. Exp. Med.* **2019**, *216* (8), 1828–1842. https://doi.org/10.1084/jem.20181970.

(90) Roston, D.; Demapan, D.; Cui, Q. Extensive Free-Energy Simulations Identify Water as the Base in Nucleotide Addition by DNA Polymerase. *Proc. Natl. Acad. Sci.* **2019**, *116* (50), 25048–25056. https://doi.org/10.1073/pnas.1914613116.

(91) Bowler, M. W.; Cliff, M. J.; Waltho, J. P.; Blackburn, G. M. Why Did Nature Select Phosphate for Its Dominant Roles in Biology? *New J. Chem.* **2010**, *34* (5), 784–794. https://doi.org/10.1039/B9NJ00718K.

(92) Jin, Y.; Cliff, M. J.; Baxter, N. J.; Dannatt, H. R. W.; Hounslow, A. M.; Bowler, M. W.; Blackburn, G. M.; Waltho, J. P. Charge-Balanced Metal Fluoride Complexes for Protein Kinase A with Adenosine Diphosphate and Substrate Peptide SP20. *Angew. Chem. Int. Ed.* **2012**, *51* (49), 12242–12245. https://doi.org/10.1002/anie.201204266.